Quelques exemples d'application aux composites stratitfiés de la théorie Bending-Gradient pour les plaques

Arthur Lebée, Karam Sab

Quelques exemples d'application aux composites stratitfiés de la théorie Bending-Gradient pour les plaques

Illustration of the Bending-Gradient plate theory applied to laminated plates

A. Lebée[1] et K. Sab[1]

1 : Université Paris-Est, Laboratoire Navier (ENPC/IFSTTAR/CNRS).
École des Ponts Paris Tech,
6 et 8 avenue Blaise Pascal.
77455 Marne-la-Vallée cedex2
e-mail : karam.sab@enpc.fr, arthur.lebee@enpc.fr

Résumé

Ce travail présente l'application aux composites fibrés d'une nouvelle théorie de plaque. Ce modèle destiné aux plaques épaisses et anisotropes utilise les six inconnues statiques de la theorie de Kirchhoff-Love auxquelles sont ajoutées six nouvelles inconnues représentant le gradient du moment de flexion. Nommé théorie Bending-Gradient, ce nouveau modèle peut être considéré comme une extension aux plaques hétérogènes dans l'épaisseurs du modèle de Reissner-Mindlin ; ce dernier étant un cas particulier lorsque la plaque est homogène. La théorie Bending-Gradient est appliquée aux plaques stratifiées et comparée à la solution exacte de Pagano [1] ainsi qu'à d'autres approches. Elle donne de bonnes prédictions pour la flèche, pour la distribution des contraintes de cisaillement transverse ainsi que pour les déplacements plans dans de nombreuses configurations matérielles.

Abstract

This work presents the application to laminated plates of a new plate theory for out-of-plane loaded thick plates where the static unknowns are those of the Kirchhoff-Love theory, to which six components are added representing the gradient of the bending moment. The Bending-Gradient theory is an extension to arbitrarily layered plates of the Reissner-Mindlin theory which appears as a special case when the plate is homogeneous. The new theory is applied to multilayered plates and its predictions are compared to full 3D Pagano's exact solutions and other approaches. It gives good predictions of both deflection, shear stress distributions and in-plane displacement distribution in many material configuration.

Mots Clés : Theorie de plaque, Modèle d'ordre supérieur, Plaque stratifiée, Plaque composite
Keywords : Plate theory, Higher-order models, Laminated plates, Composite plates

1. Introduction

Laminated plates are widely used in engineering applications. For instance angle-ply carbon fiber reinforced laminates are commonly used in aeronautics. However, these materials are strongly anisotropic and the plate overall behavior is difficult to capture. The simplest plate theory is Kirchhoff-Love plate model. However, this theory does not enable the derivation of accurate transverse shear stress distribution.

In recent decades many suggestions have been made to go further than Kirchhoff-Love model. Two main approaches can be found : asymptotic approaches and axiomatic approaches. The first one is mainly based on asymptotic expansions in the small parameter h/L [2, 3]. However, it leads to more complex models than Reissner-Mindlin model which is commonly used by engineers. The second main approach is based on assuming *ad hoc* displacement or stress 3D fields. These models can be "Equivalent Single Layer" or "Layerwise". Equivalent single layer models treat the whole laminate as an equivalent homogeneous plate. However, when dealing with laminated plates, most of these models lead to discontinuous transverse shear stress distributions through the thickness as indicated by Reddy [4]. In Layerwise models, all plate degrees of freedom are introduced in each layer of the laminate and continuity conditions are enforced between layers. The reader can refer to Reddy [4]

and Carrera [5] for detailed reviews of kinematic approaches and to [6, 7, 8] for static approaches. Layerwise models lead to correct estimates of local 3D fields. However, their main drawback is that they involve a number of degrees of freedom proportional to the number of layers.
In [9, 10] we revisited the use of 3D equilibrium in order to derive transverse shear stress as Reissner [11] did for homogeneous plates. Thanks to standard variational tools, this led to an Equivalent Single Layer plate theory which takes accurately into account shear effects and does not require any specific constitutive material symmetry : the Bending-Gradient theory. This plate theory is identical to the Reissner-Mindlin plate theory in the case of homogeneous plates. However, for laminated plates, shear forces are replaced by the gradient of the bending moment $\mathbb{R} = \mathbf{M} \otimes \boldsymbol{\nabla}$. Hence, this theory belongs to the family of higher-order gradient models. The mechanical meaning of the bending gradient was identified as self-equilibrated static unknowns associated to warping functions in addition to conventional shear forces.
The purpose of the present work is to present the application of the Bending-Gradient theory to highly anisotropic laminated plates. The paper is organized as follows. In Section 2 notations are introduced. In Section 3, the Bending-Gradient plate theory is shortly detailed. Then it is applied to fibrous laminates under cylindrical bending in Section 4 and compared with approximations based on Reissner-Mindlin theory.

2. Notations

Vectors and higher-order tensors are boldfaced and different typefaces are used for each order : vectors are slanted : $\boldsymbol{T}, \boldsymbol{u}$. Second order tensors are sans serif : $\mathbf{M}, \mathbf{e}$. Third order tensors are in typewriter style : $\mathtt{\Phi}, \mathtt{\Gamma}$. Fourth order tensors are in calligraphic style $\boldsymbol{\mathcal{D}}, \boldsymbol{\mathcal{c}}$. Sixth order tensors are double stroked $\mathbb{F}, \mathbb{W}$.
When dealing with plates, both 2-dimensional (2D) and 3D tensors are used. Thus, $\widetilde{\boldsymbol{T}}$ denotes a 3D vector and $\boldsymbol{T}$ denotes a 2D vector or the in-plane part of $\widetilde{\boldsymbol{T}}$. The same notation is used for higher-order tensors : $\widetilde{\boldsymbol{\sigma}}$ is the 3D second-order stress tensor while $\boldsymbol{\sigma}$ is its in-plane part. When dealing with tensor components, the indexes specify the dimension : $\mathtt{a}_{ij}$ denotes the 3D tensor $\widetilde{\mathbf{a}}$ with Latin index $i, j, k.. = 1, 2, 3$ and $\mathtt{a}_{\alpha\beta}$ denotes the 2D tensor $\mathbf{a}$ with Greek indexes $\alpha, \beta, \gamma.. = 1, 2$. The identity for in-plane elasticity is $i_{\alpha\beta\gamma\delta} = \frac{1}{2}\left(\delta_{\alpha\gamma}\delta_{\beta\delta} + \delta_{\alpha\delta}\delta_{\beta\gamma}\right)$, where $\delta_{\alpha\beta}$ is Kronecker's symbol. The transpose operation ${}^t\bullet$ is applied to any order tensors as follows : $({}^tA)_{\alpha\beta\ldots\psi\omega} = A_{\omega\psi\ldots\beta\alpha}$. Three contraction products are defined, the usual dot product ($\widetilde{\boldsymbol{a}} \cdot \widetilde{\boldsymbol{b}} = a_i b_i$), the double contraction product ($\widetilde{\mathbf{a}} : \widetilde{\mathbf{b}} = \mathtt{a}_{ij}\mathtt{b}_{ji}$) and a triple contraction product ($\mathtt{A} \therefore \mathtt{B} = \mathtt{A}_{\alpha\beta\gamma}\mathtt{B}_{\gamma\beta\alpha}$). Einstein's notation on repeated indexes is used in these definitions. It should be noticed that closest indexes are summed together in contraction products. The derivation operator $\widetilde{\boldsymbol{\nabla}}$ is also formally represented as a vector : $\widetilde{\mathbf{a}} \cdot \widetilde{\boldsymbol{\nabla}} = \mathtt{a}_{ij}\nabla_j = \mathtt{a}_{ij,j}$ is the divergence and $\widetilde{\mathbf{a}} \otimes \widetilde{\boldsymbol{\nabla}} = \mathtt{a}_{ij}\nabla_k = \mathtt{a}_{ij,k}$ is the gradient. Here $\otimes$ is the dyadic product. Finally, the integration through the thickness is noted $\langle\bullet\rangle : \int_{-\frac{h}{2}}^{\frac{h}{2}} f(x_3)dx_3 = \langle f \rangle$.

3. The Bending-Gradient plate theory

Summary of the plate model

We consider a linear elastic plate of thickness h which mid-plane is the 2D domain $\omega \subset \mathbb{R}^2$ (Figure 1). Cartesian coordinates (x_1, x_2, x_3) in the reference frame $(\widetilde{\boldsymbol{e}}_1, \widetilde{\boldsymbol{e}}_2, \widetilde{\boldsymbol{e}}_3)$ are used. The local stiffness tensor $C_{ijkl}(x_3)$ is assumed to be invariant with respect to translations in the (x_1, x_2) plane and the plate is loaded exclusively with the out-of-plane distributed force $\widetilde{\boldsymbol{p}} = p_3\widetilde{\boldsymbol{e}}_3$.
The membrane stress $\mathbf{N}$, the bending moment $\mathbf{M}$, and shear forces $\boldsymbol{Q}$ are related to the actual 3D local stress by the following equations :

$$\mathtt{N}_{\alpha\beta}(x_1, x_2) = \langle \sigma_{\alpha\beta} \rangle, \quad \mathtt{M}_{\alpha\beta}(x_1, x_2) = \langle x_3 \sigma_{\alpha\beta} \rangle, \quad Q_\alpha(x_1, x_2) = \langle \sigma_{\alpha 3} \rangle \qquad \text{(Eq. 1)}$$

Moreover, we introduce the gradient of the bending moment $\mathbb{R} = \mathbf{M} \otimes \boldsymbol{\nabla}$. The 2D third-order tensor $\mathbb{R}$ comply with the following symmetry : $\mathtt{R}_{\alpha\beta\gamma} = \mathtt{R}_{\beta\alpha\gamma}$. It is possible to derive shear forces $\boldsymbol{Q}$ from $\mathbb{R}$ with :

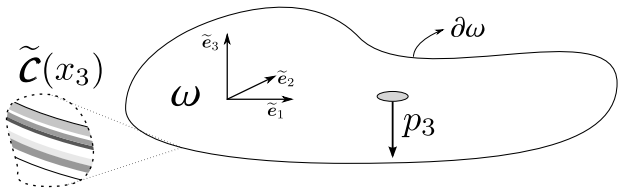

Fig. 1. The Plate Configuration

$\boldsymbol{Q} = \boldsymbol{i} \therefore \mathbb{R}$. The full bending gradient $\mathbb{R}$ has six components whereas $\boldsymbol{Q}$ has two components. Thus, using the full bending gradient as static unknown introduces four static unknowns. More precisely we have : $\mathbb{R}_{111}$ and $\mathbb{R}_{222}$ are the cylindrical bending part of shear forces Q_1 and Q_2, $\mathbb{R}_{121}$ and $\mathbb{R}_{122}$ are the torsion part of shear forces and $\mathbb{R}_{112}$ and $\mathbb{R}_{221}$ are linked to strictly self-equilibrated stresses.
Equilibrium equations and boundary conditions involving stress fields are gathered in the set of statically compatible fields :

$$\begin{cases} \mathbf{N} \cdot \boldsymbol{\nabla} = \mathbf{0} \text{ on } \omega & \text{(Eq. 2a)} \\ \mathbf{M} \otimes \boldsymbol{\nabla} - \mathbb{R} = 0 \text{ on } \omega & \text{(Eq. 2b)} \\ (\boldsymbol{i} \therefore \mathbb{R}) \cdot \boldsymbol{\nabla} = -p_3 \text{ on } \omega & \text{(Eq. 2c)} \\ \mathbf{N} \cdot \boldsymbol{n} = \boldsymbol{V}^d \text{ on } \partial\omega^s & \text{(Eq. 2d)} \\ \mathbf{M} = \mathbf{M}^d \text{ on } \partial\omega^s & \text{(Eq. 2e)} \\ (\boldsymbol{i} \therefore \mathbb{R}) \cdot \boldsymbol{n} = V_3^d \text{ on } \partial\omega^s & \text{(Eq. 2f)} \end{cases}$$

where $\partial\omega^s$ is the portion of edge on which static boundary conditions apply : $\widetilde{\boldsymbol{V}}^d$ is the force per unit length and $\mathbf{M}^d$ the full bending moment enforced on the edge. This set of equations is almost identical to Reissner-Mindlin equations where shear forces have been replaced by the bending gradient $\mathbb{R}$.
Generalized stresses $\mathbf{N}$, $\mathbf{M}$, and $\mathbb{R}$ work respectively with the associated strain variables : $\mathbf{e}$, the conventional membrane strain, $\boldsymbol{\chi}$ the curvature and $\boldsymbol{\Gamma}$ the generalized shear strain. These strain fields must comply with the following compatibility conditions and boundary conditions :

$$\begin{cases} \mathbf{e} = \boldsymbol{i} : (\boldsymbol{\nabla} \otimes \boldsymbol{U}) \text{ on } \omega & \text{(Eq. 3a)} \\ \boldsymbol{\chi} = \boldsymbol{\Phi} \cdot \boldsymbol{\nabla} \text{ on } \omega & \text{(Eq. 3b)} \\ \boldsymbol{\Gamma} = \boldsymbol{\Phi} + \boldsymbol{i} \cdot \boldsymbol{\nabla} U_3 \text{ on } \omega & \text{(Eq. 3c)} \\ \boldsymbol{\Phi} \cdot \boldsymbol{n} = \mathbf{H}^d \text{ on } \partial\omega^k & \text{(Eq. 3d)} \\ \widetilde{\boldsymbol{U}} = \widetilde{\boldsymbol{U}}^d \text{ on } \partial\omega^k & \text{(Eq. 3e)} \end{cases}$$

where $\widetilde{\boldsymbol{U}}$ is the average through the thickness of the 3D displacement of the plate and $\boldsymbol{\Phi}$ is the generalized rotation. $\boldsymbol{\Gamma}$ and $\boldsymbol{\Phi}$ are 2D third-order tensors with the following symmetry : $\Phi_{\alpha\beta\gamma} = \Phi_{\beta\alpha\gamma}$. Moreover, $\partial\omega^k$ is the portion of edge on which kinematic boundary conditions apply : $\widetilde{\boldsymbol{U}}^d$ is a given displacement and $\mathbf{H}^d$ is a symmetric second-order tensor related to a forced rotation on the edge. These fields are almost identical to Reissner-Mindlin kinematically compatible fields where the rotation pseudo-vector is replaced by the generalized rotation $\boldsymbol{\Phi}$. Assuming $\boldsymbol{\Phi} = \boldsymbol{i} \therefore \boldsymbol{\varphi}$ in Eq. 3 lead to a Reissner-Mindlin like kinematic.
Finally, for constitutive material following local monoclinic symmetry with respect to (x_1, x_2) plane (uncoupling between $\mathbb{R}$ and $(\mathbf{N}, \mathbf{M})$) the Bending-Gradient plate constitutive equations are written as :

$$\begin{cases} \mathbf{N} = \boldsymbol{\mathcal{A}} : \mathbf{e} + \boldsymbol{\mathcal{B}} : \boldsymbol{\chi} & \text{(Eq. 4a)} \\ \mathbf{M} = {}^t\boldsymbol{\mathcal{B}} : \mathbf{e} + \boldsymbol{\mathcal{D}} : \boldsymbol{\chi} & \text{(Eq. 4b)} \\ \boldsymbol{\Gamma} = \mathbb{f} \therefore \mathbb{R}, \quad \text{where}_3 \quad (\mathbb{I} - \mathbb{f} \therefore \mathbb{F}) \therefore \boldsymbol{\Gamma} = 0 & \text{(Eq. 4c)} \end{cases}$$

where conventional Kirchhoff-Love stiffnesses are defined as : $(\mathcal{A},\mathcal{B},\mathcal{D}) = \left\langle \left(1, x_3, x_3^2\right) \boldsymbol{c}(x_3) \right\rangle$ and $\boldsymbol{c}(x_3)$ is the local plane-stress stiffness tensor. The generalized shear compliance tensor $\mathbb{f}$ is a sixth order tensor :

$$\mathbb{f} = \int_{-\frac{h}{2}}^{\frac{h}{2}} \left(\int_{-\frac{h}{2}}^{x_3} \left({}^t\boldsymbol{b} + z\,\boldsymbol{d} \right) : \boldsymbol{c}(z) dz \right) \cdot \mathsf{S}(x_3) \cdot \left(\int_{-\frac{h}{2}}^{x_3} \boldsymbol{c}(z) : (\boldsymbol{b} + z\,\boldsymbol{d})\, dz \right) dx_3 \qquad \text{(Eq. 5)}$$

where $(\boldsymbol{a},\boldsymbol{b},\boldsymbol{d})$ are the Kirchhoff-Love compliances and $\mathsf{S} = \mathsf{S}_{\alpha\beta} = 4\mathcal{S}_{\alpha 3 \beta 3}$ is the out-of-plane shear compliance tensor ($\mathcal{S} = \mathcal{C}^{-1}$). Since $\mathbb{f}$ is not always invertible, we introduced Moore-Penrose pseudo inverse for the shear stiffness tensor $\mathbb{F}$:

$$\mathbb{F} = \lim_{\kappa \to 0} \left(\mathbb{f} \therefore \mathbb{f} + \kappa \mathbb{I} \right)^{-1} \therefore \mathbb{f}$$

where $\mathbb{I}$ is the identity for 2D sixth-order tensors following the generalized shear compliance $\mathbb{f}$ minor and major symmetries ($\mathbb{I}_{\alpha\beta\gamma\delta\varepsilon\zeta} = i_{\alpha\beta\varepsilon\zeta}\,\delta_{\gamma\delta}$). The solution of the plate model must comply with the three sets of equations (Eq. 2, Eq. 3, Eq. 4). The compliance $\mathbb{f}$ is positive. However when $\mathbb{f}$ is not definite, there is a set of solutions, up to a self-stress field.

Fields localization

Once the plate model is solved, it is possible to recover an approximation of local 3D fields using plate unknowns. The local stress is derived as :

$$\widetilde{\boldsymbol{\sigma}}^{BG} = \widetilde{\boldsymbol{s}}^{(\mathsf{N})} : \mathsf{N} + \widetilde{\boldsymbol{s}}^{(\mathsf{M})} : \mathsf{M} + \widetilde{\boldsymbol{s}}^{(\mathsf{R})} \therefore \mathsf{R} \qquad \text{(Eq. 6)}$$

where

$$\begin{cases} s^{(\mathsf{N})}_{\alpha\beta\varepsilon\zeta}(x_3) = c_{\alpha\beta\gamma\delta}(x_3) \left(a_{\delta\gamma\varepsilon\zeta} + x_3\, b_{\zeta\varepsilon\gamma\delta} \right) \quad \text{and } s^{(\mathsf{N})}_{i3\varepsilon\zeta} = 0 & \text{(Eq. 7a)} \\ s^{(\mathsf{M})}_{\alpha\beta\varepsilon\zeta}(x_3) = c_{\alpha\beta\gamma\delta}(x_3) \left(b_{\delta\gamma\varepsilon\zeta} + x_3\, d_{\delta\gamma\varepsilon\zeta} \right) \quad \text{and } s^{(\mathsf{M})}_{i3\varepsilon\zeta} = 0 & \text{(Eq. 7b)} \\ s^{(\mathsf{R})}_{\alpha 3\eta\zeta\varepsilon}(x_3) = -\int_{-\frac{h}{2}}^{x_3} c_{\alpha\eta\gamma\delta}(z) \left(b_{\delta\gamma\varepsilon\zeta} + z\, d_{\delta\gamma\varepsilon\zeta} \right) dz \,,\ s^{(\mathsf{R})}_{\alpha\beta\eta\zeta\varepsilon} = 0 \text{ and } s^{(\mathsf{R})}_{33\eta\zeta\varepsilon} = 0 & \text{(Eq. 7c)} \end{cases}$$

The in-plane displacement field is :

$$\boldsymbol{u}^{BG} = \boldsymbol{U} - x_3 \boldsymbol{\nabla} U_3 + \boldsymbol{\upsilon}^{(\mathsf{R})} \therefore \mathsf{R} \qquad \text{(Eq. 8)}$$

where

$$\upsilon^{(\mathsf{R})}_{\alpha} = \int_{-\frac{h}{2}}^{x_3} \mathsf{S}_{\alpha\zeta}(z) s^{(\mathsf{R})}_{\zeta 3\beta\gamma\delta}(z) dz + k^{(\mathsf{R})}_{\alpha\beta\gamma\delta} \qquad \text{(Eq. 9)}$$

and the fourth order tensor $\boldsymbol{k}^{(\mathsf{R})}$ is an integration constant chosen such as $\left\langle u^{(\mathsf{R})}_{\alpha} \right\rangle = 0$.

4. Application to laminates

4.1. Plate configuration

We consider angle-ply laminates. Each ply is made of unidirectional fiber-reinforced material oriented at θ relative to Direction x_1. All plies have the same thickness and are perfectly bounded. A laminate is denoted between brackets by the successive ply-orientations along thickness. For instance $[0^\circ, 90^\circ]$ denotes a 2-ply laminate where the lower ply fibers are oriented in the bending direction. The constitutive behavior of a ply is assumed to be transversely isotropic along the direction of the fibers and engineering constants are chosen similar to those of Pagano [1] :

$$E_L = 25 \times 10^6 psi, \quad E_T = 1 \times 10^6 psi, \quad G_{LT} = 0.5 \times 10^6 psi, \quad G_{TT} = 0.4 \times 10^6 psi,$$
$$\nu_{LT} = \nu_{TT} = 0.25$$

where G_{TT} has been changed to preserve transversely isotropic symmetry. L is the longitudinal direction oriented in the (x_1, x_2) plane at θ with respect to $\widetilde{\boldsymbol{e}}_1$, T is the transverse direction.

4.2. Cylindrical bending

Pagano [1] gives an exact solution for cylindrical bending of simply supported composite laminates. We choose the same configuration for the Bending-Gradient model. The plate is invariant and infinite in x_2 direction. It is out-of-plane loaded with $p_3(x_1) = -p_0 \sin \kappa x_1$. The plate is simply supported at $x_1 = 0$ and $x_1 = L$ with traction free edges.
NB : Pagano [1, 12, 13] derived exact 3D elasticity solution of this problem for a laminate loaded only on the upper face and free on the lower face. In the present work we assume the plate is identically loaded on its upper and lower face to comply with the plate model [9] : $T_3^+ = T_3^- = \frac{p_3}{2}$ where $T_3^{\pm}$ is the normal traction on the upper and lower face of the plate.
Closed-form solutions using the Bending-Gradient and the Reissner-Mindlin model were derived. For the latter, the work of Whitney [14] was used for deriving transverse shear stress distributions. Shear correction factors were taken into account into the shear constitutive equation of the Reissner-Mindlin plate model.
A comparison with a finite elements solution was also performed on ABAQUS [15]. Since the Bending-Gradient is an Equivalent Single Layer theory, conventional shell elements were chosen (3 displacements and 3 rotations). Transverse shear fields with shell elements in ABAQUS are derived using an approach very similar to Whitney [14] where it is furthermore assumed that the plate overall constitutive equation is orthotropic with respect to the main bending direction. *S*4, linear quadrangle with full integration elements, were used. A convergence test was performed. This study enforced the typical size of an element $l_{char} = h/5$ where h is the plate thickness. For instance when the slenderness is $h/L = 1/4$ there are 20 elements. Finally, section integration is performed during the analysis.

4.3. Results

We consider first a symmetric cross ply $[0°, 90°, 0°, 90°, 0°, 90°, 0°, 90°, 0°]$ laminate. In this case, the plate configuration fulfills the assumptions made for the finite elements approximation (orthotropic laminate). In Figure 2, shear stress distribution at $x_1 = 0$ in Direction 1 is plotted for the exact solution from Pagano [1] : $\boldsymbol{\sigma}^{Ex}$, the Bending-Gradient solution : $\boldsymbol{\sigma}^{(\mathrm{R})}$, Whitney's shear distribution : $\boldsymbol{\sigma}^{(Q),W}$ and the finite elements solution : $\boldsymbol{\sigma}^{(Q),FE}$. The slenderness ratio is set to $L/h = 4$ as conventionally done when benchmarking plate models. The three approximate solutions yield the same distribution. The discrepancy with the exact solution is well-known and associated to edge effects.
In Figure 3 is plotted the in-plane displacement at $x_1 = 0$ in Direction 1. The displacement is normalized with the mid-span Kirchhoff-Love deflection, U_3^{KL}. The Bending-Gradient approximation follows closely the exact solution.
In Figure 4 the mid-span deflection error is plotted versus the slenderness ratio for the Bending-Gradient solution (*BG*), the finite elements solution (RM, FE) and the closed-form Reissner-Mindlin solution (RM, WE). Kirchhoff-Love deflection is also plotted as reference. This error is defined as : $\Delta(U_3) = \frac{U_3^{Ex}(L/2) - U_3(L/2)}{U_3^{Ex}(L/2)}$, where $U_3^{Ex}(x_1)$ is the plate deflection taken for the exact solution. The three approximate solutions yield almost the same error.
Now we take the initial 9-ply configuration and simply rotate it 45° with respect to the bending direction. It becomes a symmetric and non-orthotropic $[45°, -45°, 45°, -45°, 45°, -45°, 45°, -45°, 45°]$ laminate. This configuration does not comply with the assumptions made for the finite elements approach. In Figure 6 shear distributions are compared to the exact solution. The Bending-Gradient solution remains close to the exact solution. However finite elements and Whitney's solution yield a different distribution which is not as accurate as the Bending-Gradient. More precisely, in Direction 2, the FE solution does not capture the change of slope associated to the change of ply orientation.
In Figure 7 is plotted the in-plane displacement in both directions. The Bending-Gradient approximation matches accurately the exact solution. Especially, in Direction 2 the distribution follows a Zig-Zag shape. Thus the Bending-Gradient approximation is able to capture this well-known feature

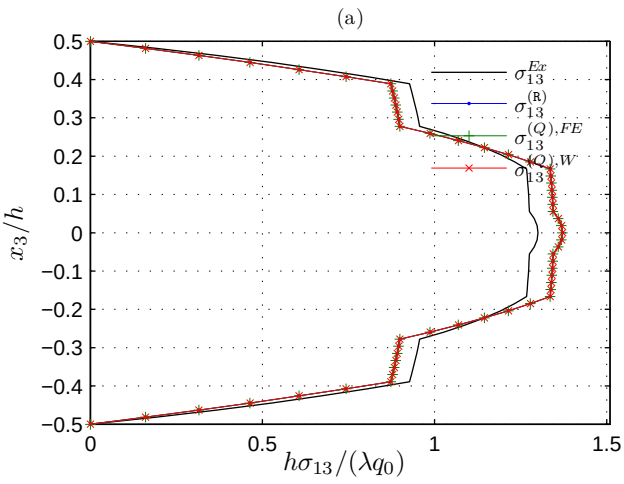

Fig. 2. Normalized shear distribution σ_{13} *at* $x_1 = 0$ *for a* $[0°,90°,0°,90°,0°,90°,0°,90°,0°]$ *laminate,* $L/h = 4$*,* ($\sigma_{23} = 0$ *: symmetry).*

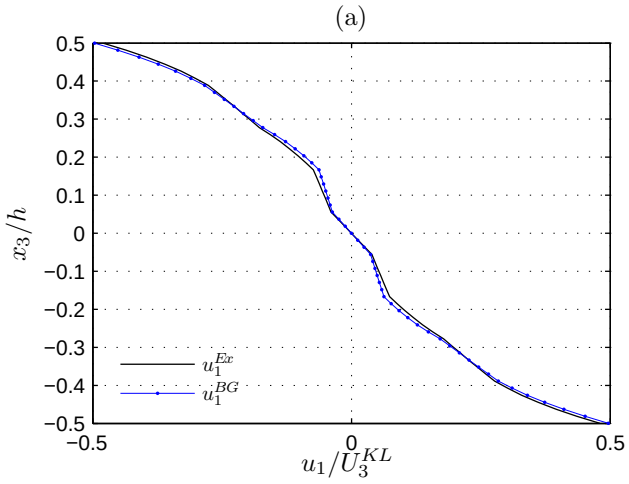

Fig. 3. In-plane displacement distribution u_1 *at* $x_1 = 0$ *for a* $[0°,90°,0°,90°,0°,90°,0°,90°,0°]$ *laminate,* $L/h = 4$*,* ($u_2 = 0$ *: symmetry).*

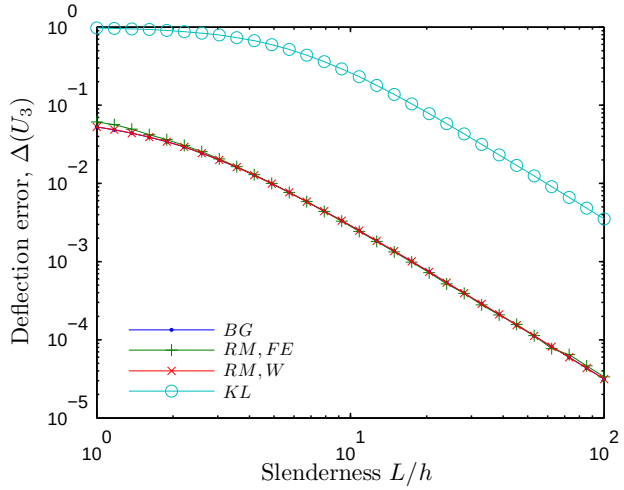

Fig. 4. Deflection error versus slenderness ratio for a $[0°,90°,0°,90°,0°,90°,0°,90°,0°]$ *laminate (BG : Bending-Gradient, RM,FE : finite elements, RM,W :[14], KL : Kirchhoff-Love)*

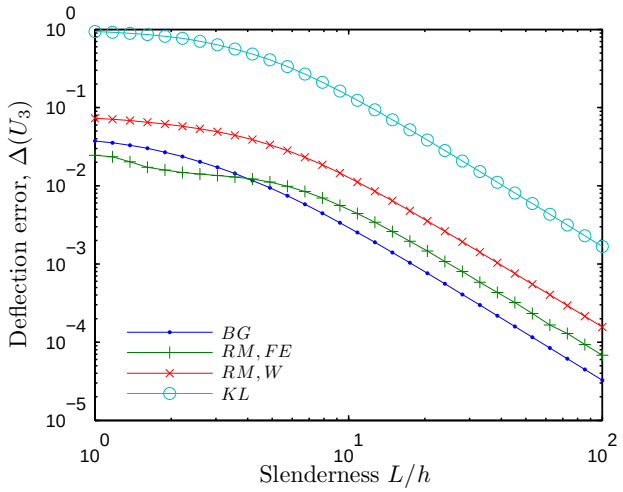

Fig. 5. Deflection error versus slenderness ratio for a $[45°,-45°,45°,-45°,45°,-45°,45°,-45°,45°]$ *laminate*

of laminates displacement fields. In Figure 5 the mid-span deflection error is plotted versus the slenderness ratio. The Bending-Gradient solution is the most accurate one for conventional slenderness.

4.4. Discussion

We have numerically compared three approaches for deriving an approximation of the exact solution for cylindrical bending suggested by Pagano [1, 12, 13] applied to a symmetric cross-ply configuration in two bending directions.

The first main observation which comes out of this analysis is the critical influence of the assumption of orthotropy with respect to the bending direction. When this assumption is fullfilled, the three approximations lead to almost identical results. Otherwise, both Whitney's and Finite Element approximations lead to poor estimation of transverse shear stress distribution and deflection. In the case of finite elements this is because we do not respect the assumption of the model. In the case of Whitney [14], the main reason for this discrepancy comes from the assumption of cylindrical bending. This assumption neglects the influence of the pure warping unknowns included in the bending gradient :

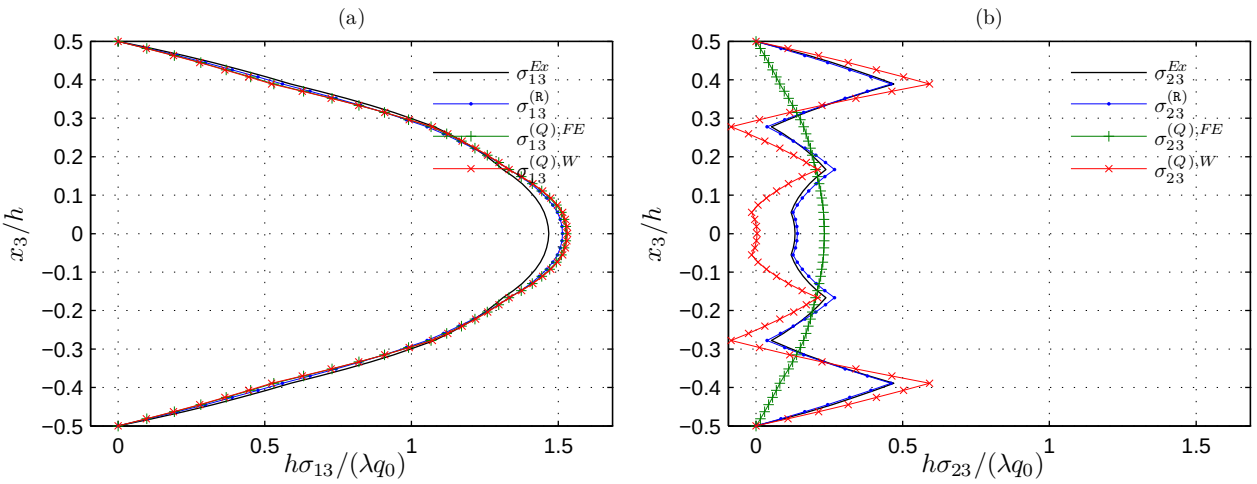

Fig. 6. Normalized shear distribution in both directions at $x_1 = 0$ for a $[45°, -45°, 45°, -45°, 45°, -45°, 45°, -45°, 45°]$ laminate, $L/h = 4$, a) σ_{13} b) σ_{23}.

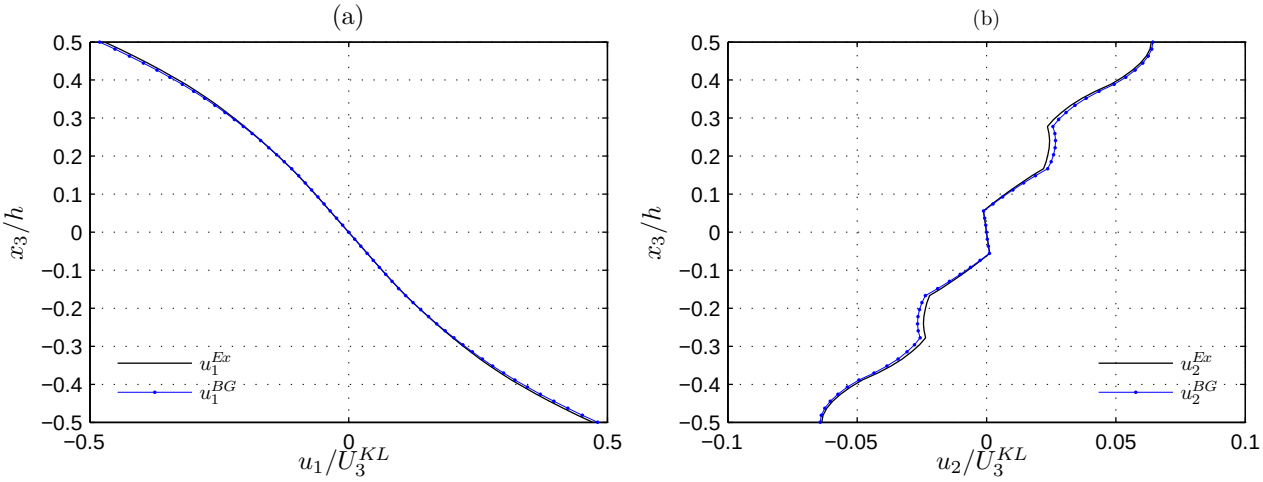

Fig. 7. In-plane displacement distribution at $x_1 = 0$ for a $[45°, -45°, 45°, -45°, 45°, -45°, 45°, -45°, 45°]$ laminate, $L/h = 4$, a) u_1 b) u_2.

$\mathbf{R}_{112}$ and $\mathbf{R}_{221}$ and generates the difference in shear stress distribution and therefore in deflection.
The second observation is that a simple rotation of the plate with respect to the bending direction leads to very different transverse shear stress distribution. This shows clearly the necessity to distinguish between torsion and cylindrical bending components in the gradient of the bending moment. In most plate models they are mixed into shear forces ($Q_1 = \mathbf{R}_{111} + \mathbf{R}_{122}$) whereas the components $\mathbf{R}_{111}$ and $\mathbf{R}_{122}$ lead to different transverse shear stress distributions. This explains the significant difference when changing the bending direction. More generally, this raises the question of the relevence of benchmarking plate models in configurations where only the cylindrical part of the bending gradient is involved (assuming orthotropy with respect to the bending direction is a typical example) whereas laminated plate engineering applications involves much more general configurations.
Finally, the Bending-Gradient solution was presented for a plate which follows mirror symmetry. This model gives a very good approximation of both local and macroscopic fields at a rather low computational cost (no post-process integration through the thickness and Reissner-Mindlin-like partial derivative equations).
When the laminate is not mirror-symmetric, the Bending-Gradient gives less accurate results (details are given in [10]) : the transverse shear distribution or the related in-plane displacement might not exactly converge to the exact solution but still leads to good approximation. Several explanations are

currently under investigation. Especially, the contribution to the stress energy of the membrane stress gradient, $\mathbf{N} \otimes \nabla$ was ignored when deriving the Bending-Gradient model. Neglecting this contribution explains the discrepancy when the membrane stress in not zero, which occurs when the plate is not mirror-symmetric.

5. Conclusion

In the present work we provided first applications using the Bending-Gradient plate theory. Closed-form solutions for cylindrical bending were applied to laminates and compared to Reissner-Mindlin and finite elements approximations. The main conclusion is that the Bending-Gradient gives good predictions of both deflection and shear stress distributions in many material configuration especially when the plate is mirror-symmetric.
Several outlooks are under consideration. First, this plate theory can be extended to periodic plates such as sandwich panels [16, 17]. Second, the estimation of the influence of the membrane stress gradient on the quality of the shear stress estimation will be studied in detail.

Références

[1] N. Pagano « Exact Solutions for Composite Laminates in Cylindrical Bending », *Journal of Composite Materials* Vol. 3 n° 3, pp. 398–411, 1969.

[2] D. Caillerie « Thin elastic and periodic plates. », *Mathematical Methods in the Applied Sciences* Vol. 6 n° 2, pp. 159 – 191, 1984, ISSN 01704214.

[3] T. Lewinski « Effective Models Of Composite Periodic Plates .3. 2-Dimensional Approaches », *International Journal Of Solids And Structures* Vol. 27 n° 9, pp. 1185–1203, 1991.

[4] J. N. Reddy « On Refined Computational Models Of Composite Laminates », *International Journal For Numerical Methods In Engineering* Vol. 27 n° 2, pp. 361–382, 1989.

[5] E. Carrera « Theories and finite elements for multilayered, anisotropic, composite plates and shells », *Archives Of Computational Methods In Engineering* Vol. 9 n° 2, pp. 87–140, 2002.

[6] A. Diaz Diaz, J.-F. Caron, R. P. Carreira « Model for laminates », *Comptes Rendus de l'Académie des Sciences - Series IIB - Mechanics* Vol. 329 n° 12, pp. 873–879, 2001, ISSN 1620-7742.

[7] J. F. Caron, A. D. Diaz, R. P. Carreira, A. Chabot, A. Ehrlacher « Multi-particle modelling for the prediction of delamination in multi-layered materials », *Composites Science And Technology* Vol. 66 n° 6, pp. 755–765, 2006.

[8] A. Diaz Diaz, J. F. Caron, A. Ehrlacher « Analytical determination of the modes I, II and III energy release rates in a delaminated laminate and validation of a delamination criterion », *Composite Structures* Vol. 78 n° 3, pp. 424–432, 2007.

[9] A. Lebée, K. Sab « A bending gradient model for thick plates, Part I : Theory », submitted .

[10] A. Lebée, K. Sab « A bending gradient model for thick plates, Part II : Closed-form solutions for cylindrical bending », submitted .

[11] E. Reissner « The effect of transverse shear deformation on the bending of elastic plates », *Journal of Applied Mechanics* Vol. 12, pp. 68–77, 1945.

[12] N. Pagano « Exact Solutions for Rectangular Bidirectional Composites and Sandwich Plates », *Journal of Composite Materials* Vol. 4 n° 1, pp. 20–34, 1970.

[13] N. Pagano « Influence of Shear Coupling in Cylindrical. Bending of Anisotropic Laminates », *Journal of Composite Materials* Vol. 4 n° 3, pp. 330–343, 1970.

[14] J. Whitney « Stress Analysis of Thick Laminated Composite and Sandwich Plates », *Journal of Composite Materials* Vol. 6 n° 4, pp. 426–440, 1972.

[15] ABAQUS, ABAQUS/Standard user's manual, version 6.7, 2007.

[16] A. Lebée, K. Sab « Reissner-Mindlin Shear Moduli of a Sandwich Panel with Periodic Core Material », in : Mechanics of Generalized Continua, vol. 21 of *Advances in Mechanics and Mathematics*, Springer New York, , pp. 169–177, 2010.

[17] A. Lebée, K. Sab « Transverse shear stiffness of a chevron folded core used in sandwich construction », *International Journal of Solids and Structures* Vol. 47 n° 18-19, pp. 2620–2629, 2010, ISSN 0020-7683.